Possible Inversion Symmetry Breaking in the $S = 1/2$ Pyrochlore Heisenberg Magnet

Imre Hagymási,[1,2,*] Robin Schäfer,[1,†] Roderich Moessner,[1,‡] and David J. Luitz[1,§]
[1]*Max Planck Institute for the Physics of Complex Systems, Noethnitzer Strasse 38, 01187 Dresden, Germany*
[2]*Strongly Correlated Systems "Lendület" Research Group, Institute for Solid State Physics and Optics, Wigner Research Centre for Physics, Budapest H-1525 P.O. Box 49, Hungary*

(Received 13 October 2020; accepted 12 February 2021; published 18 March 2021)

We address the ground-state properties of the long-standing and much-studied three-dimensional quantum spin liquid candidate, the $S = \frac{1}{2}$ pyrochlore Heisenberg antiferromagnet. By using SU(2) density-matrix renormalization group (DMRG), we are able to access cluster sizes of up to 128 spins. Our most striking finding is a robust spontaneous inversion symmetry breaking, reflected in an energy density difference between the two sublattices of tetrahedra, familiar as a starting point of earlier perturbative treatments. We also determine the ground-state energy, $E_0/N_{\text{sites}} = -0.490(6)J$, by combining extrapolations of DMRG with those of a numerical linked cluster expansion. These findings suggest a scenario in which a finite-temperature spin liquid regime gives way to a symmetry-broken state at low temperatures.

DOI: 10.1103/PhysRevLett.126.117204

Introduction.—Frustrated magnets, on account of exhibiting many competing low energy states, are a fertile ground for exotic physics. A celebrated example is the pyrochlore Heisenberg antiferromagnet, which resides on a lattice of corner sharing tetrahedra, depicted in the inset of Fig. 1. The classical Heisenberg model on this lattice has a highly degenerate ground state [1], forming a classical spin liquid [2] with an emergent gauge field [3].

In contrast, the ground state of the quantum pyrochlore antiferromagnet remains enigmatic. While recent experimental evidence in the approximately isotropic $S = 1$ compound $NaCaNi_2F_7$ shows a spin liquid like state down to low temperature [31], the $S = 1/2$ case is still open both in theory and experiment.

Theory work on this prominent quantum spin liquid candidate over the years has been formidable. Absent a systematically controlled method, various approaches have somewhat inevitably led to an array of possible scenarios. One strand of work has built on a perturbative approach, in which half the couplings (those on one tetrahedral sublattice) are switched on perturbatively. This has led to suggestions of a ground state which breaks translational and rotational symmetries [7,32,33], a valence bond crystal [10] or a spin liquid state [34]. On top of this, the contractor renormalization method [35] finds antiferromagnetic ordering in a space of supertetrahedral pseudospins, pointing to

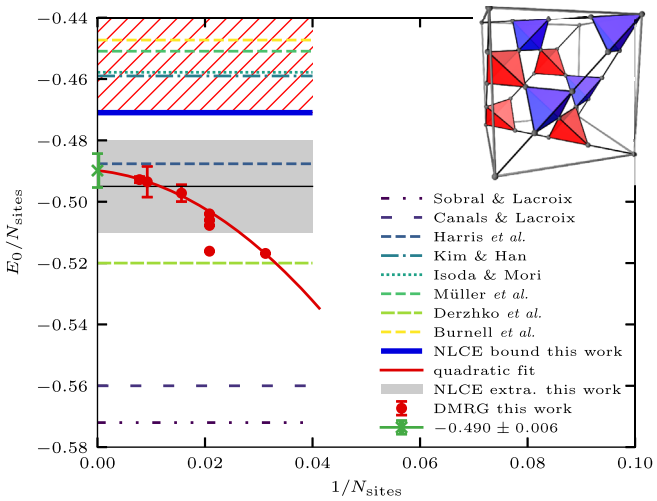

FIG. 1. Ground-state energies from various approaches. The horizontal lines denote the predictions for the ground-state energy per site ($J = 1$) in the thermodynamic limit: Sobral and Lacroix −0.572 [4], Canals and Lacroix −0.56 [5], Derzhko *et al.* −0.52 [6], Harris *et al.* −0.487 [7,8], Kim and Han −0.459, [9], Isoda and Mori −0.4578 [10], Müller *et al.* −0.4509 [11], Burnell *et al.* −0.4473 [12]. The solid red points are our DMRG results for periodic clusters, extrapolated to infinite bond dimension using a quadratic polynomial. The thick blue line represents a robust upper bound for the ground-state energy, obtained from converged NLCE results at finite temperature, thus excluding the red hashed area. The solid black line shows the extrapolated value of the converged NLCE results to zero temperature (cf. Supplemental Material [13]), and the gray shaded area indicates the confidence interval of this extrapolation. The inset shows the cubic unit cell of the pyrochlore lattice, highlighting the two tetrahedral sublattices in red and blue.

an even larger real-space unit cell. To render the problem more tractable, all these theories involve the derivation of an effective Hamiltonian, which is *per se* not exactly solvable and hence solved by some type of approximation, ranging from mean field theory to classical Monte Carlo numerics. On a different axis in theory space, parton-based theories yield an ordered state with a chiral order parameter [9] or a monopole flux state [12], while the pseudofermion functional renormalization group suggests a spin liquid ground state [36].

In view of this relatively wide range of ground-state candidates, a controlled and unbiased treatment of the model is clearly desirable, if only to narrow the possible location of the goalposts somewhat. Unfortunately, most numerical approaches quickly reach their limits for frustrated magnets in $d = 3$. While exact diagonalization is currently limited to ∼48 sites [37], possible alternatives are series expansions such as the numerical linked cluster expansion (NLCE) [14–30] or high temperature expansions [38,39], which can be pushed down to low temperatures [30], although they do not provide access to the ground state itself and are particularly challenged by many competing low energy states.

To access the ground-state wave function directly, the density-matrix renormalization group (DMRG) method—originally devised in one dimension [40–44]—has been pushed to two dimensions, in particular for the two-dimensional cousin of pyrochlore, the kagome antiferromagnet [45–49].

Here, we take DMRG one step further, by applying it to the pyrochlore lattice in $d = 3$, and present a study of periodic clusters with $N_{\text{sites}} = 32, 48, 64, 108, 128$. This demonstrates that DMRG can treat clusters with up to 128 sites reliably, significantly larger than previous exact diagonalization results of 36 sites [50]. Exploiting the SU(2) symmetry of the model [51–54], we keep up to 20 000 SU(2) states, (typically equivalent to $\gtrsim$80 000 U(1) states). We calculate the ground-state energy, the spin structure factor, and low-energy excitations for these clusters, yielding an estimate for the ground-state energy per site in the thermodynamic limit of $E_0/N_{\text{sites}} = -0.490(6)$. The study of finite size clusters is complemented by a high order NLCE calculation, which *excludes* any scenario where $E_0/N_{\text{sites}} > -0.471$.

Our main finding is that the ground state of the larger (64-, 108-, and 128-site) clusters we consider exhibits a breathing instability, rendering up and down tetrahedra (cf. inset of Fig. 1) inequivalent: one tetrahedral sublattice exhibits a lower energy than the other. Amusingly, our estimate for the ground state energy is compatible with that of the original perturbation theory with a simple mean field solution of the resulting effective Hamiltonian, where the inversion symmetry was maximally broken at the very outset of the calculation [7].

Model and methods.—We consider the $S=1/2$ pyrochlore antiferromagnetic Heisenberg model, $H=J\sum_{\langle i,j\rangle}\vec{S}_i\cdot\vec{S}_j$, where the spins sit on the sites i, j of the 3D pyrochlore lattice and $\langle i,j\rangle$ denotes nearest neighbors. The lattice is a face centered cubic lattice with lattice vectors $\vec{a}_1 = \frac{1}{2}(1,1,0)^T$, $\vec{a}_2 = \frac{1}{2}(1,0,1)^T$, $\vec{a}_3 = \frac{1}{2}(0,1,1)^T$, and a tetrahedral basis given by $\vec{b}_0 = \vec{0}$, $\vec{b}_1 = \frac{1}{2}\vec{a}_1$, $\vec{b}_2 = \frac{1}{2}\vec{a}_2$, $\vec{b}_3 = \frac{1}{2}\vec{a}_3$, such that each lattice point can be expressed by $\vec{R}_{\alpha,n_1,n_2,n_3} = n_1\vec{a}_1 + n_2\vec{a}_2 + n_3\vec{a}_3 + \vec{b}_\alpha$, with integer n_1, n_2, n_3 and $\alpha \in \{0,1,2,3\}$. The model is obviously SU(2) symmetric. Our DMRG calculations are performed on finite size ($N = 32, 48, 64, 108, 128$) clusters with periodic boundary conditions (cf. Supplemental Material [13]).

We apply the one- and two-site variants of SU(2) DMRG to reach the high bond dimensions necessary to obtain reliable results in our three-dimensional clusters. Since DMRG requires a one-dimensional topology, we impose a one-dimensional "snake" path on the three-dimensional lattice, which defines the variational manifold. We use fully periodic clusters to reduce boundary effects and confirm that using a snake path which minimizes the bandwidth of the connectivity matrix improves convergence [30,55,56].

For small bond dimensions ($\chi \lesssim 2000$) we use the two-site version of the DMRG, and switch to the one-site variant to optimize the wave function for larger χ. Since the truncation error is not well defined in the one-site variant case (due to the subspace expansion [53]), we use the reliable two-site variance estimation to extrapolate towards the error-free case [57], because calculation of the full variance would be impractical due to its cost.

It turns out that even the calculation of the two-site variance becomes too costly for clusters with more than ∼100 sites and bond dimensions $\gtrsim$8000. In certain cases, we revert to the usage of the two-site DMRG and extrapolate as a function of the truncation error (cf. 108-site cluster).

Ground-state energy.—Using DMRG, we calculate the variational ground-state energy of finite clusters with high accuracy. By systematically increasing the bond dimension χ, we enlarge the variational manifold in a controlled way, such that we can extrapolate, $\chi \to \infty$, to the exact limit using a linear extrapolation as a function of the two-site variance (cf. Fig. 2). We use an estimate of the systematic extrapolation error given by half the distance between the extrapolated value and the last DMRG point.

Figure 1 shows the extrapolated energies per lattice site of all finite clusters we considered in comparison with the available predicted ground-state energies in the literature. Our results show a monotonic growth of the ground-state energy as the number of sites is increased.

The periodic clusters we consider have either the full cubic (32, 108) or an increased or reduced (48*a*, 48*b*, 48*c*, 48*d*, 64, 128) symmetry of the pyrochlore lattice and represent the bulk due to the absence of a surface. The energies per site of different clusters as a function of inverse

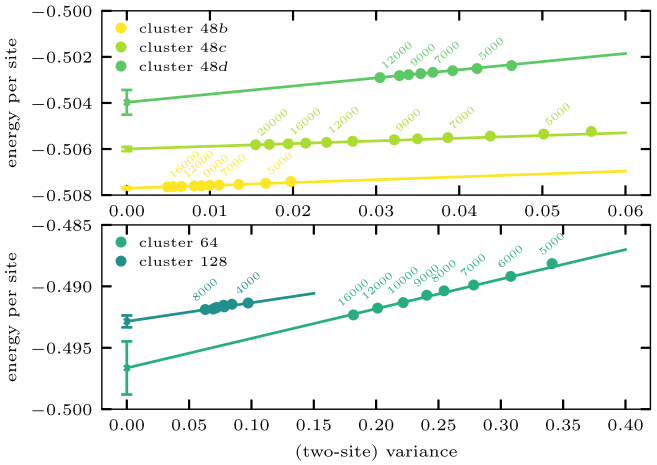

FIG. 2. Variational ground state energy estimates of the clusters 48*b*, 48*c*, 48*d* (top) and 64,128 (bottom) for different bond SU(2) bond dimensions χ (indicated by the labels) as a function of the two-site variance. Solid lines correspond to linear extrapolations to the error-free limit, corresponding to infinite bond dimension and zero variance. We estimate the systematic extrapolation error as the half distance between the last point and the extrapolated value.

cluster size admit a fit to a quadratic polynomial, which we use to obtain an extrapolation to the thermodynamic limit. In order to get an estimate of the extrapolation error, we use Gaussian resampling, using the systematic DMRG error bars as standard deviation. This yields our best estimate for the ground-state energy of $E_0/N_{\text{sites}} = -0.490(6)$. In this fit we considered only the cluster 48*d* among the 48-site clusters, which appears to be consistent with the other clusters, while other 48-site clusters have lower ground-state energies.

Our extrapolated ($\chi \to \infty$) cluster energies and gaps are summarized in Table I. While the singlet gaps in the most symmetric clusters (32, 48*d*) are very small, the triplet gaps are sizable and roughly an order of magnitude larger. Since the 48*d* cluster does not obey all lattice symmetries, a reliable extrapolation is not possible, but our results are compatible with a scenario with a finite triplet gap, in which case all low energy excitations would be in the singlet sector as claimed in Refs. [32,35].

Our finite temperature NLCE [14–30] provides a complementary perspective. We have carried out this expansion in entire tetrahedra up to eighth order (cf. Ref. [30] for details, as well as the Supplemental Material [13]), obtaining convergence for the energy per site in the thermodynamic limit as a function of temperature for temperatures $T \gtrsim 0.2$. Since the energy is a monotonic function of temperature, the converged part of $E(T)$ (cf. Supplemental Material [13]) provides an upper bound for the ground-state energy $E_{\text{NLCE}} \approx -0.471J$, which is consistent with the DMRG data and extrapolation. One can furthermore polynomially extrapolate the finite temperature

TABLE I. Ground-state energies per site and gaps within the $S_{\text{tot}} = 0$ sector (singlet gap) as well as to the $S_{\text{tot}} = 1$ sector (triplet gap) if available.

Cluster	GS energy	Singlet gap	Triplet gap
32	−0.5168	0.0318	0.6872
48*a*	−0.5161	0.2166(4)	0.6709(4)
48*b*	−0.5077	0.027(2)	0.554(2)
48*c*	−0.5060(1)	0.053(7)	0.42(2)
48*d*	−0.5040(5)	0.06(3)	0.36(3)
64	−0.4972(25)		
108	−0.4935(50)		
128	−0.4928(10)		

NLCE energies to zero temperature (assuming an analytic behavior at low temperatures), see Supplemental Material [13], and obtain −0.495(15), which agrees remarkably well with the DMRG extrapolation and lies within its error bar, serving as a further corroboration of the DMRG energy. In light of these results we can confidently exclude a ground-state energy per site larger than $-0.47J$.

Ground-state symmetry breaking.—To investigate the properties of the ground state in more detail, we calculate the total spin, and hence total energy, of up and down tetrahedra separately. This reveals an inequivalence of up and down tetrahedra (cf. Supplemental Material [13]), suggesting a breaking of the inversion symmetry of the lattice. In our DMRG calculations, the snake path does not fully respect the symmetry between up and down tetrahedra, so we need to verify that this symmetry breaking is intrinsic, and not due to a preference imposed by the snake path. We therefore introduce a small symmetry breaking "breathing" perturbation, where we modify the couplings of up and down tetrahedra to be $J = 1 \pm \epsilon$, equivalent to the standard technique of including pinning fields.

Figure 3 shows the results for the total spin of up and down tetrahedra for opposite signs of the breathing

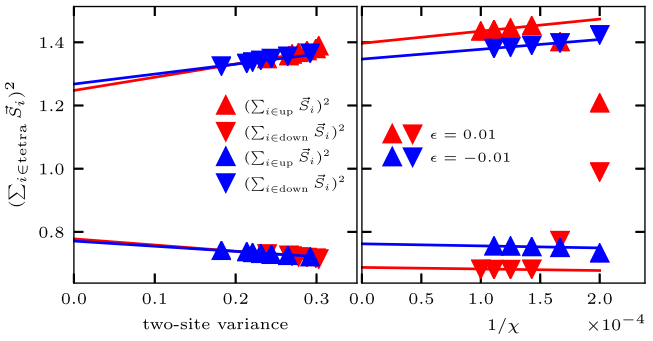

FIG. 3. Extrapolation of tetrahedron spins for an explicit breaking of lattice inversion symmetry, similarly to a "pinning" coupling, for the 64 (left) and 108 (right) site clusters. The whole Hamiltonian is written as $H = (1-\epsilon)H_{\text{up}} + (1+\epsilon)H_{\text{down}}$, where the H_{up} and H_{down} parts contain the terms for the up and down tetrahedra, respectively.

perturbation in the 64 (108) site clusters as a function of the two-site variance (inverse bond dimension), admitting a linear extrapolation towards $\chi \to \infty$. The results reveal a clear selection of states with opposite symmetry breaking, as required for spontaneous symmetry breaking. The order parameters for the larger, 108-site, cluster are slightly different for the two opposite pinning fields (Fig. 3, right panel), but that difference is much smaller than the extrapolated order parameter which differs only little between the two clusters. It is of course always possible in principle that the symmetry breaking vanishes when yet larger clusters are considered. Given the scaling of the computational effort with system size, the study of much larger clusters with the present method is, however, out of reach. In the Supplemental Material [13] we provide further evidence that the two symmetry-breaking states converge to the same energy after the pinning field is removed.

We next consider nearest neighbor spin correlations of the best (lowest-energy) wave functions $|\psi_0\rangle$ obtained in DMRG. For each pair of adjacent sites (i, j), we calculate the correlation function $C_{ij} = \langle\psi_0|\vec{S}_i \cdot \vec{S}_j|\psi_0\rangle$. We plot the result for the clusters 64 and 128 in Fig. 4 (truncated to the cubic unit cell for ease of visualization), with the tube thickness proportional to the strength of the spin correlations.

The correlation pattern reveals that one sublattice (say, "up") of tetrahedra contains more strongly correlated bonds than the other. These are found on opposite edges of up tetrahedra. We note that the details of this pattern still depend strongly on the cluster geometry and we get opposite choices of correlated bonds in the two clusters, presumably due to different symmetry broken states picked by the different "snake" paths in the two clusters. Moreover, the periodic boundary conditions impact the performance of the DMRG calculation. In particular, finite-sized clusters with periodic boundary conditions comprise winding loops which may be as short as, or even shorter, than the "physical" loops in the bulk, whose minimal length is the circumference, 6, of a hexagon. Resonances along both loop types will therefore compete. The minimal length of winding loops for $N = 108$ is 6 while it is 8 for $N = 128$. Indeed, we observe considerably better convergence for the latter, inducing a smaller error, see Fig. 1. The shortest periodic loop of each cluster is shown in the Supplemental Material [13].

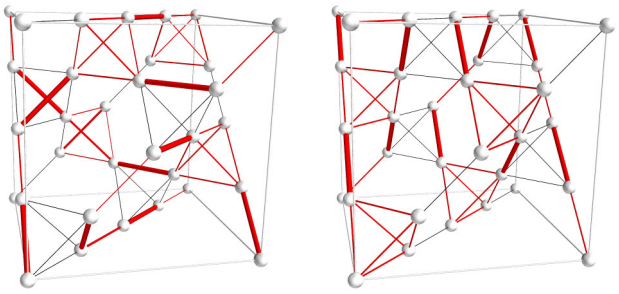

FIG. 4. Real space spin correlation C_{ij} in the ground state ($S_z = 0$) for $N = 64$ (left) and $N = 128$ (right) shown in the cubic unit cell. The thickness of the red bonds corresponds to magnitude of the correlation between neighboring sites. The black lines indicate bonds between sites with negligible correlations.

Ground-state structure factor.—The static spin structure factor for different clusters, accessible in neutron scattering experiments, is obtained from the Fourier transform of the spin correlations [factor 4/3 from normalization $1/(S(S+1))$ for spin $S = 1/2$]:

$$S(\vec{Q}) = \frac{4}{3N}\sum_{ij}\langle\vec{S}_i \cdot \vec{S}_j\rangle_c \cos\left[\vec{Q} \cdot (\vec{R}_i - \vec{R}_j)\right], \qquad (1)$$

where $\vec{R}_i$ denote the real-space coordinates of sites and the index c denotes the connected part of the correlation matrix. The results for two cuts [$Q_x = Q_y$ (top) and $Q_z = 0$ (bottom)] in the three-dimensional momentum space are shown in Fig. 5.

One can readily recognize the bow-tie patterns, the hallmark of pyrochlore magnets [3,7,11,30,31,34,36]. Note that the 32- and 108-site clusters have full cubic symmetry, while the 64-site cluster does not, hence the structure factors looks slightly different in that case. The results for the spin structure factor and the absence of sharp Bragg peaks confirm that there is no long range magnetic ordering. The observed pattern for the $Q_x = Q_y$ cuts is very close to what is found at finite temperature in the regime $T \lesssim 1$ [30], on the other hand the $Q_z = 0$ cuts exhibit a drastic change in the 108- and 128-site clusters reflecting the symmetry breaking. While the pinch points sharpen with increasing system size (and therefore momentum resolution), we are unable to extrapolate their width reliably to the thermodynamic limit to extract a correlation length.

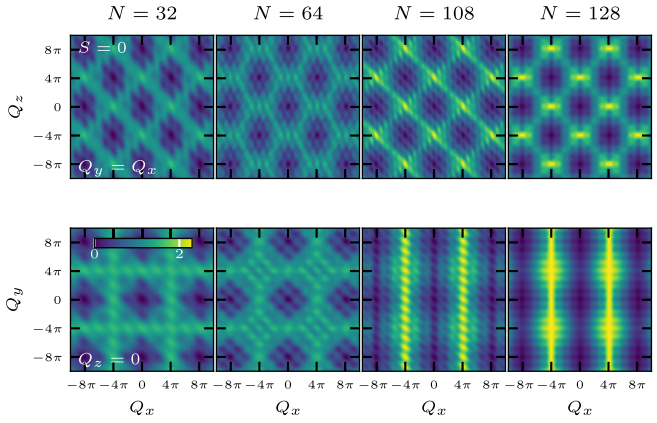

FIG. 5. Static spin structure factor for different clusters for two cuts [$Q_x = Q_y$ (top) and $Qz = 0$ (bottom)] through momentum space. The corresponding maximal bond dimensions for the 32, 64, 108, and 128-site clusters are 20 000,16 000, 16 000, and 12 000, respectively.

Note that for the largest clusters, apparent lines in the spin structure factor in the Q_x-Q_y plane become discernible, Fig. 4, raising the possibility of at least short-range spin correlations with spatial anisotropy. A more detailed search for such symmetry breaking is clearly warranted.

Concluding discussion.—Our DMRG study has found the ground state of the SU(2) symmetric $S = \frac{1}{2}$ Heisenberg antiferromagnet to discard lattice inversion symmetry in favor of a "breathing" pattern of strong (weak) sublattices of up (down) tetrahedra. We extrapolate the energy per lattice site to $-0.490(6)$. The possibility of such *spontaneous* symmetry breaking has been a central question for this class of magnets, as several studies have used an *explicit* such symmetry breaking as a starting point of various perturbative schemes [7,32,35,58]. As the restoration of an explicitly broken symmetry in a perturbative scheme is generically not to be expected, a nonvanishing order parameter does not *per se* indicate spontaneous symmetry breaking.

Our results are thus important in that they provide largely unbiased evidence for the existence of this spontaneous symmetry breaking, subject only to finite-size effects which are much reduced in comparison to previous studies. This also indicates that one of the prime Heisenberg quantum spin liquid candidates in three dimensions in fact exhibits at least one form of symmetry breaking.

In closing, we note that our extrapolated ground-state energy lies close to the estimate obtained in the pioneering work by Harris *et al.* [7], in the abovementioned scheme of coupling the up tetrahedra perturbatively through the bonds of the down tetrahedra. These authors also found a long-range dimer ordering (cf. also Ref. [32]) compatible with the correlation pattern we observe in our calculations shown in Fig. 4. This first, simple and quite uncontrolled, approach to this difficult problem thus may turn out to have been already quite close to what will eventually be established as the final answer.

We thank Owen Benton, Ludovic Jaubert, Paul McClarty, Jeffrey Rau, Johannes Richter, Oleg Derzhko, Masafumi Udagawa, and Karlo Penc for very helpful discussions. We acknowledge financial support from the Deutsche Forschungsgemeinschaft through SFB 1143 (Project-id 247310070) and cluster of excellence ct.qmat (EXC 2147, Project-id 390858490). I. H. was supported in part by the Hungarian National Research, Development and Innovation Office (NKFIH) through Grants No. K120569 and No. K134983. Some of the data presented here was produced using the SyTen toolkit, originally created by Claudius Hubig [51,52].

*hagymasi@pks.mpg.de
†schaefer@pks.mpg.de
‡moessner@pks.mpg.de
§dluitz@pks.mpg.de

[1] J. Villain, Insulating spin glasses, Z. Phys. B **33**, 31 (1979).
[2] R. Moessner and J. T. Chalker, Properties of a Classical Spin Liquid: The Heisenberg Pyrochlore Antiferromagnet, Phys. Rev. Lett. **80**, 2929 (1998).
[3] S. V. Isakov, K. Gregor, R. Moessner, and S. L. Sondhi, Dipolar Spin Correlations in Classical Pyrochlore Magnets, Phys. Rev. Lett. **93**, 167204 (2004).
[4] R. R. Sobral and C. Lacroix, Order by disorder in the pyrochlore antiferromagnets, Solid State Commun. **103**, 407 (1997).
[5] B. Canals and C. Lacroix, Quantum spin liquid: The Heisenberg antiferromagnet on the three-dimensional pyrochlore lattice, Phys. Rev. B **61**, 1149 (2000).
[6] O. Derzhko, T. Hutak, T. Krokhmalskii, J. Schnack, and J. Richter, Adapting Planck's route to investigate the thermodynamics of the spin-half pyrochlore Heisenberg antiferromagnet, Phys. Rev. B **101**, 174426 (2020).
[7] A. B. Harris, A. J. Berlinsky, and C. Bruder, Ordering by quantum fluctuations in a strongly frustrated Heisenberg antiferromagnet, J. Appl. Phys. **69**, 5200 (1991).
[8] A. Koga and N. Kawakami, Frustrated Heisenberg antiferromagnet on the pyrochlore lattice, Phys. Rev. B **63**, 144432 (2001).
[9] J. H. Kim and J. H. Han, Chiral spin states in the pyrochlore Heisenberg magnet: Fermionic mean-field theory and variational Monte Carlo calculations, Phys. Rev. B **78**, 180410 (R) (2008).
[10] M. Isoda and S. Mori, Valence-Bond Crystal and Anisotropic Excitation Spectrum on 3-Dimensionally Frustrated Pyrochlore, J. Phys. Soc. Jpn. **67**, 4022 (1998).
[11] P. Müller, A. Lohmann, J. Richter, and O. Derzhko, Thermodynamics of the pyrochlore-lattice quantum Heisenberg antiferromagnet, Phys. Rev. B **100**, 024424 (2019).
[12] F. J. Burnell, S. Chakravarty, and S. L. Sondhi, Monopole flux state on the pyrochlore lattice, Phys. Rev. B **79**, 144432 (2009).
[13] See Supplemental Material at http://link.aps.org/supplemental/10.1103/PhysRevLett.126.117204 for more details, which includes Refs. [14–30].
[14] M. Rigol, T. Bryant, and R. R. P. Singh, Numerical Linked-Cluster Approach to Quantum Lattice Models, Phys. Rev. Lett. **97**, 187202 (2006).
[15] M. Rigol, T. Bryant, and R. R. P. Singh, Numerical linked-cluster algorithms. II. $t-j$ models on the square lattice, Phys. Rev. E **75**, 061119 (2007).
[16] M. Rigol, T. Bryant, and R. R. P. Singh, Numerical linked-cluster algorithms. I. Spin systems on square, triangular, and Kagomé lattices, Phys. Rev. E **75**, 061118 (2007).
[17] E. Khatami and M. Rigol, Thermodynamics of the antiferromagnetic Heisenberg model on the checkerboard lattice, Phys. Rev. B **83**, 134431 (2011).
[18] E. Khatami, J. S. Helton, and M. Rigol, Numerical study of the thermodynamics of clinoatacamite, Phys. Rev. B **85**, 064401 (2012).
[19] E. Khatami, R. R. P. Singh, and M. Rigol, Thermodynamics and phase transitions for the Heisenberg model on the pinwheel distorted Kagome lattice, Phys. Rev. B **84**, 224411 (2011).
[20] E. Khatami and M. Rigol, Thermodynamics of strongly interacting fermions in two-dimensional optical lattices, Phys. Rev. A **84**, 053611 (2011).

[21] E. Khatami and M. Rigol, Effect of particle statistics in strongly correlated two-dimensional Hubbard models, Phys. Rev. A **86**, 023633 (2012).

[22] R. Applegate, N. R. Hayre, R. R. P. Singh, T. Lin, A. G. R. Day, and M. J. P. Gingras, Vindication of $Yb_2Ti_2O_7$ as a Model Exchange Quantum Spin Ice, Phys. Rev. Lett. **109**, 097205 (2012).

[23] R. R. P. Singh and J. Oitmaa, Corrections to Pauling residual entropy and single tetrahedron based approximations for the pyrochlore lattice Ising antiferromagnet, Phys. Rev. B **85**, 144414 (2012).

[24] B. Tang, E. Khatami, and M. Rigol, A short introduction to numerical linked-cluster expansions, Comput. Phys. Commun. **184**, 557 (2013).

[25] N. R. Hayre, K. A. Ross, R. Applegate, T. Lin, R. R. P. Singh, B. D. Gaulin, and M. J. P. Gingras, Thermodynamic properties of $Yb_2Ti_2O_7$ pyrochlore as a function of temperature and magnetic field: Validation of a quantum spin ice exchange Hamiltonian, Phys. Rev. B **87**, 184423 (2013).

[26] L. D. C. Jaubert, O. Benton, J. G. Rau, J. Oitmaa, R. R. P. Singh, N. Shannon, and M. J. P. Gingras, Are Multiphase Competition and Order by Disorder the Keys to Understanding $Yb_2Ti_2O_7$? Phys. Rev. Lett. **115**, 267208 (2015).

[27] O. Benton, L. D. C. Jaubert, R. R. P. Singh, J. Oitmaa, and N. Shannon, Quantum Spin Ice with Frustrated Transverse Exchange: From a π-Flux Phase to a Nematic Quantum Spin Liquid, Phys. Rev. Lett. **121**, 067201 (2018).

[28] O. Benton, Instabilities of a U(1) Quantum Spin Liquid in Disordered Non-Kramers Pyrochlores, Phys. Rev. Lett. **121**, 037203 (2018).

[29] T. Pardini, A. Menon, S. P. Hau-Riege, and R. R. P. Singh, Local entanglement and confinement transitions in the random transverse-field Ising model on the pyrochlore lattice, Phys. Rev. B **100**, 144437 (2019).

[30] R. Schäfer, I. Hagymási, R. Moessner, and D. J. Luitz, Pyrochlore $S = \frac{1}{2}$ Heisenberg antiferromagnet at finite temperature, Phys. Rev. B **102**, 054408 (2020).

[31] K. W. Plumb, H. J. Changlani, A. Scheie, S. Zhang, J. W. Krizan, J. A. Rodriguez-Rivera, Y. Qiu, B. Winn, R. J. Cava, and C. L. Broholm, Continuum of quantum fluctuations in a three-dimensional $S = 1$ Heisenberg magnet, Nat. Phys. **15**, 54 (2019).

[32] H. Tsunetsugu, Spin-singlet order in a pyrochlore antiferromagnet, Phys. Rev. B **65**, 024415 (2001).

[33] H. Tsunetsugu, Antiferromagnetic quantum spins on the pyrochlore lattice, J. Phys. Soc. Jpn. **70**, 640 (2001).

[34] B. Canals and C. Lacroix, Pyrochlore Antiferromagnet: A Three-Dimensional Quantum Spin Liquid, Phys. Rev. Lett. **80**, 2933 (1998).

[35] E. Berg, E. Altman, and A. Auerbach, Singlet Excitations in Pyrochlore: A Study of Quantum Frustration, Phys. Rev. Lett. **90**, 147204 (2003).

[36] Y. Iqbal, T. Müller, P. Ghosh, M. J. P. Gingras, H. O. Jeschke, S. Rachel, J. Reuther, and R. Thomale, Quantum and Classical Phases of the Pyrochlore Heisenberg Model with Competing Interactions, Phys. Rev. X **9**, 011005 (2019).

[37] A. M. Läuchli, J. Sudan, and R. Moessner, $S = \frac{1}{2}$ Kagome Heisenberg antiferromagnet revisited, Phys. Rev. B **100**, 155142 (2019).

[38] A. Lohmann, H.-J. Schmidt, and J. Richter, Tenth-order high-temperature expansion for the susceptibility and the specific heat of spin-s Heisenberg models with arbitrary exchange patterns: Application to pyrochlore and Kagome magnets, Phys. Rev. B **89**, 014415 (2014).

[39] J. Richter and R. Steinigeweg, Combining dynamical quantum typicality and numerical linked cluster expansions, Phys. Rev. B **99**, 094419 (2019).

[40] S. R. White, Density Matrix Formulation for Quantum Renormalization Groups, Phys. Rev. Lett. **69**, 2863 (1992).

[41] S. R. White, Density-matrix algorithms for quantum renormalization groups, Phys. Rev. B **48**, 10345 (1993).

[42] R. M. Noack, S. R. Manmana, A. Avella, and F. Mancini, Diagonalization and numerical renormalizationgroupbased methods for interacting quantum systems, AIP Conf. Proc. **789**, 93 (2005).

[43] U. Schollwöck, The density-matrix renormalization group in the age of matrix product states, Ann. Phys. (Amsterdam) **326**, 96 (2011), january 2011 Special Issue.

[44] K. A. Hallberg, New trends in density matrix renormalization, Adv. Phys. **55**, 477 (2006).

[45] S. Depenbrock, I. P. McCulloch, and U. Schollwöck, Nature of the Spin-Liquid Ground State of the $S = \frac{1}{2}$ Heisenberg Model on the Kagome Lattice, Phys. Rev. Lett. **109**, 067201 (2012).

[46] H.-C. Jiang, Z. Wang, and L. Balents, Identifying topological order by entanglement entropy, Nat. Phys. **8**, 902 (2012).

[47] S. Yan, D. A. Huse, and S. R. White, Spin-liquid ground state of the $S = \frac{1}{2}$ Kagome Heisenberg antiferromagnet, Science **332**, 1173 (2011).

[48] Y.-C. He, M. P. Zaletel, M. Oshikawa, and F. Pollmann, Signatures of Dirac Cones in a DMRG Study of the Kagome Heisenberg Model, Phys. Rev. X **7**, 031020 (2017).

[49] H. C. Jiang, Z. Y. Weng, and D. N. Sheng, Density Matrix Renormalization Group Numerical Study of the Kagome Antiferromagnet, Phys. Rev. Lett. **101**, 117203 (2008).

[50] V. R. Chandra and J. Sahoo, Spin-$\frac{1}{2}$ Heisenberg antiferromagnet on the pyrochlore lattice: An exact diagonalization study, Phys. Rev. B **97**, 144407 (2018).

[51] C. Hubig, F. Lachenmaier, N.-O. Linden, T. Reinhard, L. Stenzel, A. Swoboda, and M. Grundner, The SyTen toolkit.

[52] C. Hubig, Symmetry-protected tensor networks, Ph. D. thesis, LMU München, 2017, https://doi.org/10.5282/edoc.21348.

[53] C. Hubig, I. P. McCulloch, U. Schollwöck, and F. A. Wolf, Strictly single-site DMRG algorithm with subspace expansion, Phys. Rev. B **91**, 155115 (2015).

[54] I. P. McCulloch, From density-matrix renormalization group to matrix product states, J. Stat. Mech. (2007) P10014.

[55] U. Schollwöck, The density-matrix renormalization group, Rev. Mod. Phys. **77**, 259 (2005).

[56] J. Ummethum, J. Schnack, and A. M. Luchli, Large-scale numerical investigations of the antiferromagnetic Heisenberg icosidodecahedron, J. Magn. Magn. Mater. **327**, 103 (2013).

[57] C. Hubig, J. Haegeman, and U. Schollwöck, Error estimates for extrapolations with matrix-product states, Phys. Rev. B **97**, 045125 (2018).

[58] R. Moessner, S. L. Sondhi, and M. O. Goerbig, Quantum dimer models and effective Hamiltonians on the pyrochlore lattice, Phys. Rev. B **73**, 094430 (2006).